ORIGINAL PAPER

GIS-based assessment of debris flow hazards in Kulekhani Watershed, Nepal

Bhuwani Paudel[1] · Mamadou Fall[1] · Bahram Daneshfar[1,2]

Abstract

Debris flows are a hazardous natural calamity in mountainous regions of Nepal. Torrential rainfall within a very short period of the year is the main triggering factor for instability of slopes and initiation of landslides in these regions. Furthermore, the topography of the mountains and poor land use practices are additional factors that contribute to these instabilities. In this research, a GIS model has been developed to assess the debris flow hazard in mountainous regions of Nepal. Landslide-triggering threshold rainfall frequency is related to the frequency of landslides and the debris flow hazard in these mountains. Rainfall records from 1980 to 2013 are computed for one- to seven-day cumulative annual maximum rainfall. The expected rainfall for 1 in 10 to 1 in 1000 years of return periods is analyzed. The expected threshold rainfall is modeled in the GIS environment to identify the factor of safety of mountain slopes in a study watershed. A relation between the frequency of rainfall and debris flow hazard area is derived for return periods of 25, 50, 100, and 200 years. The debris flow hazard results from the analysis are compared with a known event in the watershed and found to agree. This method can be applied to anticipated rainfall-induced debris flow from the live rainfall record to warn the hazard-prone community in these mountains.

Keywords Landslides · Debris flow · Hazard assessment · Himalaya · Rainfall

1 Introduction

Rainfall-induced landslides that often change into debris flows are highly hazardous in mountainous Nepal. Nepal has diverse seasonal rainfall. Approximately 80% of annual rainfall occurs in the monsoon season (June to September) alone. The majority of land is mountainous terrain (almost 83%), and 67% of the total population live in these landslide-prone mountains. Landslides were the second most common cause of human death after epidemics in Nepal from 1971 to 2015 (Ministry of Home, Nepal 2015).

✉ Mamadou Fall
mfall@uottawa.ca

1   Department of Civil Engineering, University of Ottawa, 161 Colonel By, Ottawa, ON K1N 6N5, Canada

2   Agriculture and Agri-Food Canada, 960, Carling Avenue, Ottawa, ON K1A 0C6, Canada

From 1983 to 2016, the total number of deaths and missing from landslides (particularly debris flows) was 9,153. This represents 269 lives lost per year (Ministry of Home 2016). Landslide leads to flooding in the lower part of the mountains that killed on an average 729 people per year between 1971 and 2016 (Ministry of Home, Nepal 2015; DWIDP 2017). Landslide and flooding destroyed about 5337 houses per year during the period from 1971 to 2014 (DWIDP 2017). The plain area of Nepal, which is about 17% of the total land in lower watersheds, is affected and damaged by flooding and debris flow following rainfall-induced landslide (Ministry of Home, Nepal 2015). The loss of life and property is increasing every year as suitable land is unable to match the needs of the growing population for safe residential and commercial premises. This effect is further worsened by the unplanned use of land for various activities and infrastructure development. Because of limited resources and lack of understanding, the vulnerability to landside hazard and other hazard loss is at a high level in Nepal, as pointed by Corominas et al. (2014), compared to other developing countries. Assessment of hazard, vulnerability, and risk for development activities is not a common practice, as it is hindered by a lack of understanding of debris flow initiation, inundation, and its associated hazards. It is obvious from the facts above that the prediction of the spatial distribution of debris flow hazards is important to save lives and property in Nepalese mountainous regions. However, debris flow hazard assessment on a watershed scale has not yet been studied in these mountainous regions. There is a need to address this research and technology gap to reduce the vulnerability of the population and infrastructure in these regions to debris and save life as well as to establish suitable land use plans.

The overall objective of this research is to develop models for landslide (debris flow) hazard assessment for Nepal's mountains. For landslide hazard assessment in a study area, knowledge of the temporal and spatial distribution of landslides for a given rainfall return period is necessary. Models of landslide initiation and debris flow assessment for different rainfall amounts in these mountains have been studied by Paudel (2018). As a further step toward discovering landslide hazards, research on the probability of rainfall and its effect on the spatial distribution of landslides for different return periods will be assessed. Finally, a model for hazard assessment will be developed, and it will be employed for developing hazard maps of the study area.

2 Study area

The area chosen for this study is the Kulekhani watershed, located in central Nepal, about 30 km south of the capital city, Kathmandu (Fig. 1). The size of the watershed is approximately 124 km². The details (geographical and geomorphological characteristics, geological and geotechnical characteristics, climate, land use pattern) of the watershed are available in Paudel (2018), Kayastha et al. (2013), Dhital (2003), Dhakal et al. (2000) and Lamichhanne (2000). The study watershed was devastated in 1993 by a landslide event that took the lives of 1138 people in a single incident in the region. This landslide event was associated with extreme rainfall, which triggered more than 300 landslides, most of which changed into debris flows over a two-day period, July 19 and 20, 1993. The landslide event caused flooding in the lower watershed of the river system, and the total number of recorded deaths was more than 1500 (Dhital 2003).
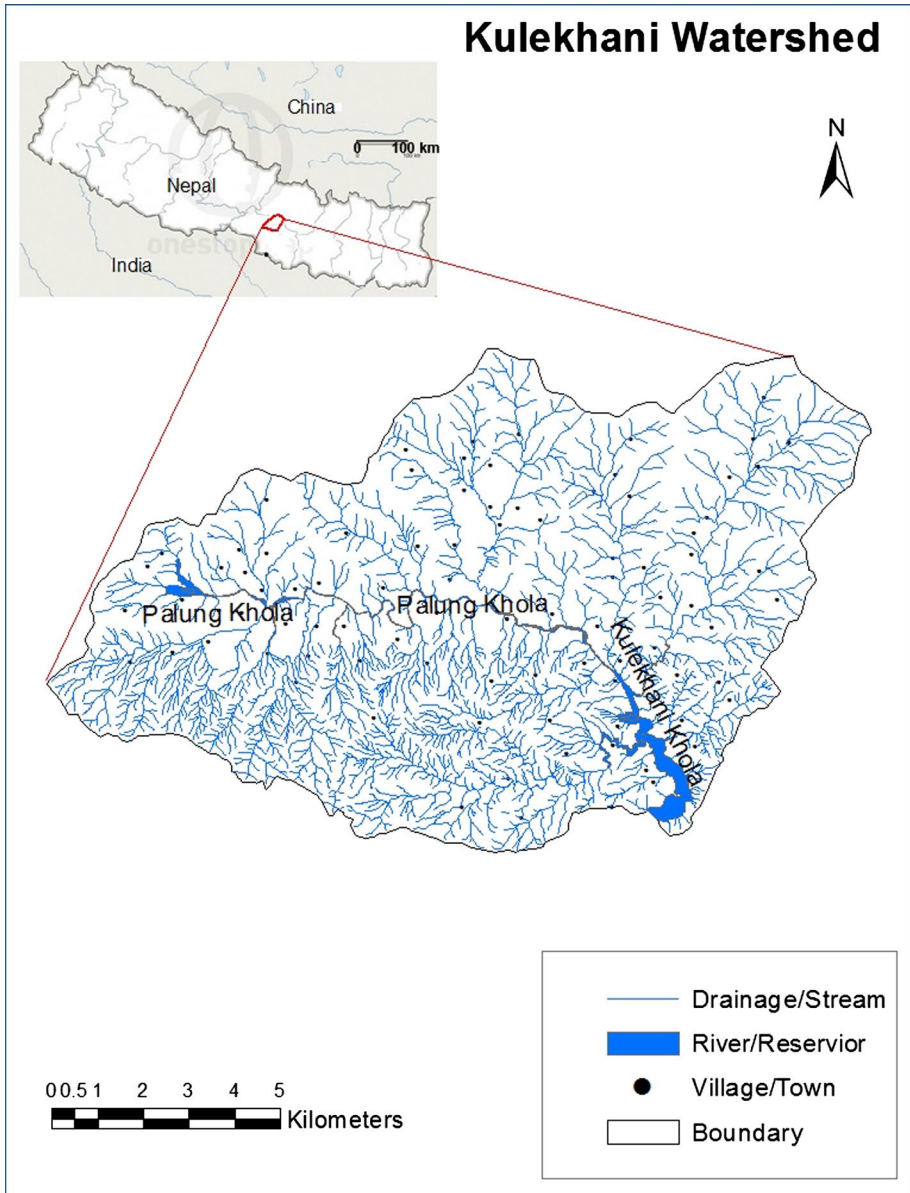
Fig. 1 Location of the study area, Kulekhani, Nepal

3 Methodology

A landslide hazard, as defined by Varnes et al. (1984), is "a probability of occurrence of a potentially damaging event in a given area and period of time." After 15 years of Varnes et al.'s work, Guzzetti et al. (1999) further defined landslide hazard by adding "magnitude" and redefining the probability of occurrence of a given magnitude of landslide in a

given duration and location. Therefore, it is important to consider three components: probability of occurrence of a landside, its location, and its size when one conducts landslide hazard assessment. Fall (2009a, b) and Fall et al. (2006) further clarified the term, stating that landslide hazard is characterized by "its location, intensity (magnitude), frequency and probability." The probability of the landside initiation, debris flow inundation, and the magnitude of the event to cause vulnerability to the element at risk are important factors for landslide hazard and risk assessment.

In this paper, the model for the "hazard" is established by applying landslide-triggering threshold rainfall duration, intensity, and annual probability (Corominas et al. 2014; Guzzetti 2005a, b). Paudel (2018) verified the critical rainfall intensity and durations for landside initiation while studying these mountains. These combinations of duration and intensity of rainfall with their return period (annual probability) are applied to obtain the probability of landslide-susceptible areas. This method is applied to the study watershed area to estimate the potential locations of probable landslide occurrence regions for a given rainfall return period. The relation of landslide area and rainfall return period is derived for different rainfall recurrence within the watershed to use in hazard analysis, as proposed by Reid and Page (2003).

Many models for landslide hazard assessments are GIS-based statistical methods, which use previous landslide events as a base factor for the identification of potential landslides in the future (Jaiswal 2011; Remondo et al. 2008). However, when a landslide occurs, the topography of the area changes, and a similar rainfall intensity and duration may not still be the threshold rainfall, even though its recurrence period is the same. When one landslide event occurs, new analysis is required to consider the associated morphological change. A model that can consider physical features of the watershed during landslide-triggering threshold rainfall is necessary for finding potential landslide locations, independent of previous events. By using rainfall events, determination of related landslide-susceptible areas, debris flow inundation, and the probability of hazard are carried out in a GIS environment in this research. The outcome is the identification of the phenomenon that makes particular hill slopes severely unstable for a given annual probable rainfall intensity and duration, and its application to hazard analysis

Figure 2 shows the methodology developed for the assessment of debris flow hazard in the study area, as well as the relationship between the different work steps of the investigations carried out. This approach includes four main stages. The first stage consists of the acquisition of data and development of the database, which are required to conduct the work described in the other stages of this study. In the second stage of this investigation, a GIS-based assessment of landslide susceptibility and probability in the study area is performed. The frequency of annual maximum rainfall is analyzed, and their related landslide events in temporal and spatial dimension are derived for the study watershed. These landslide locations are considered as debris flow sources or debris flow initiation points. The third stage deals with the GIS-based assessment of debris flow runout. The debris flow runout distances are modeled from the identified landslide initiation points. This assessment results in the development of a debris flow inundation map of the study area. Finally, in the fourth stage of this study, the results obtained in stages 2 and 3 are used to conduct a GIS-based assessment of debris flow hazards to develop a debris flow hazard map for the study area. The main stages are described in detail below.
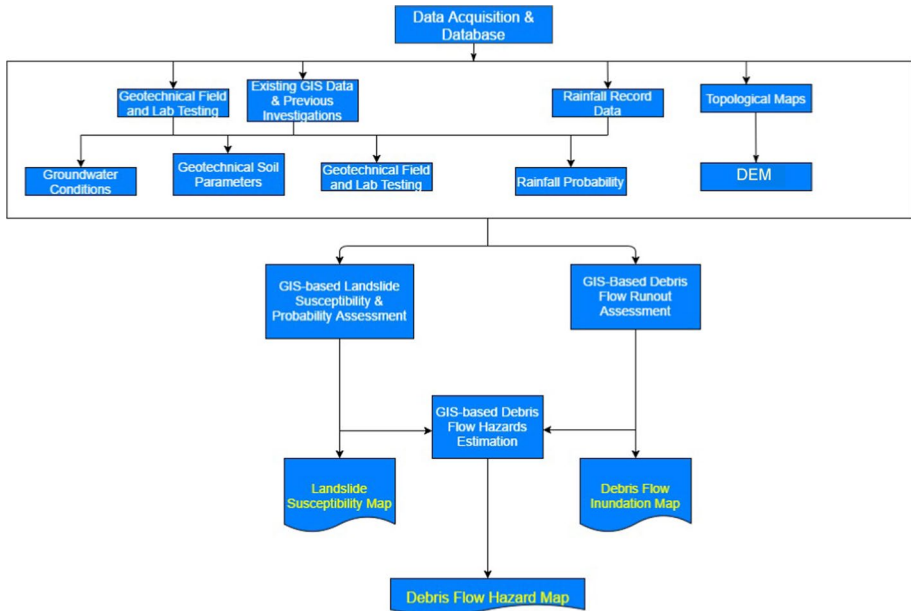
Fig. 2 Landslide (debris flow) hazard analysis methodology. *GIS* geographical information system, *DEM* digital elevation model

3.1 Data acquisition and database

Data required for this study include: (i) a topographical map of the study area that was obtained from the Topographical Survey of Nepal. Digital elevation model (DEM) was then developed from the topographical map. Slope maps were developed from the DEM as shown in Fig. 3; (ii) a geological map and previous landslide location maps, which were collected from previous research in the study watershed (Paudel 2018; Kayastha et al. 2013; Lamichhanne 2000); (iii) geotechnical parameters of the soils present in the study area. These geotechnical parameters were obtained from the results of the field and laboratory investigations performed in this study as well as from previous geotechnical investigations in the study area (Paudel 2018; Lamichhanne 2000); (iv) rainfall data from the Department of Hydrology and Meteorology of Nepal; (v) soil–water characteristic curves (SWCCs) developed from the above information.

3.1.1 Rainfall data

In the study watershed, rainfall is recorded at four rain gauge stations. Two rainfall recording gauge stations, Daman and Markhu (Fig. 3), are within the watershed and two, Chisapani and Thankot, are located close to it. Among these four rain gauge stations, the rainfall recorded in Chisapani is the highest. Rainfall is recorded once in each 24-hour period for all of these stations. The rainfall data are available for the period from 1980 to 2013. As Chisapani Ghadi rain gauge station received the maximum
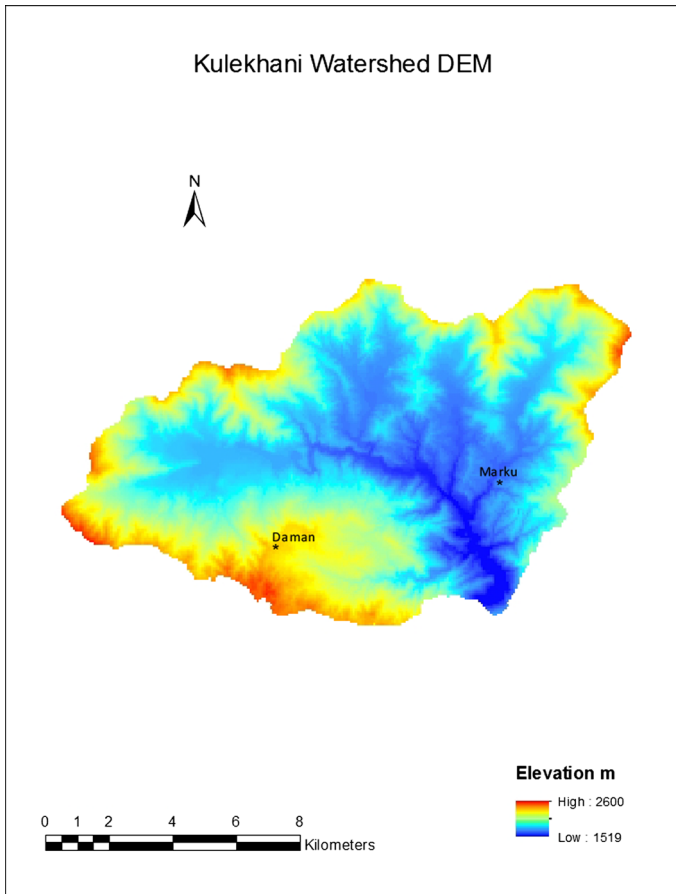
Fig. 3 Digital elevation model (DEM) for the study watershed, Kulekhani

rainfall of the four stations, this station is considered for finding the worst conditions for rainfall-induced landside hazard in the study watershed.

From the daily recorded rainfall during the period 1980 to 2013, the maximum rainfall for one-day to seven-day periods is analyzed. These series of rainfall are used for probability analysis. The probability of rainfall for one to seven days, and the consequences for landslide susceptibility are derived.

3.1.2 Topographical map and DEM

The topographical map is modeled as a triangulated irregular network (TIN) to develop DEM, a raster map, as shown in Fig. 3. Figure 3 is further used for developing slope maps. Maps of all parameters are developed in the GIS environment. All individual maps are interpolated using inverse distance weighted (IDW) methods to create continuous raster maps for the whole watershed. The extent of these maps and their cell numbers is sized to the same scale for raster analysis.

3.1.3 Groundwater conditions

There is no stable groundwater table in the hill portions of the studied watershed that can affect the slope stability in these higher mountains, although the annual average rainfall from four rain gauge stations is 1813 mm. The groundwater flow pattern and its significance for landslides in this watershed can be found in Deoja et al. (1991). Some natural water springs are found in the lower part of the watershed, but those pass through the rock faults. A temporary perched water table develops and moves downward based on the intensity and duration of rainfall. There is no stable groundwater table in the hill slope that influences the slope stability in higher mountains in Nepal. A water table is available in deeper locations in the valley which have no to very mild slopes; therefore, groundwater effects are not considered in the analysis.

3.1.4 Geotechnical data

One previous landslide area was selected to conduct geotechnical investigations in order to gain additional data (e.g., cohesion and friction angle, representing soil strength parameters) for the geotechnical characterization of the study area. The cohesion and friction angle were obtained from direct shear testing (IS: 2720–1985). On-site infiltration tests were conducted on two boreholes to ascertain infiltration capacity and permeability of in situ soils. The initial moisture content, saturated moisture content, saturated unit weight, dry unit weight, specific gravity, void ratio, grain size distribution, and saturated cohesion and friction angle were obtained from collected samples. Other watershed information of the study area is given in Dhital (2003).

The observed infiltration (0.00,178 cm/sec) is very high as compared to normal rainfall intensity in the area. For infiltration depth computation, rainfall intensity is used as the permeability coefficient in the analysis for low-intensity rainfall, and the infiltration rate is used for higher-intensity rainfall. Therefore, the observed infiltration rate was used as the permeability coefficient for the infiltration depth computation for high-intensity rainfall. The maximum wetting depth is observed for a longer duration during recorded high rainfall, as infiltration is very high.

GIS layers representing each parameter required for Eq. (14) are developed and analyzed in the GIS environment.

3.1.5 Soil–water characteristic curve (SWCC)

A total of 73 locations in the watershed were considered for SWCC development. Soil grain size distribution, plasticity index, and natural moisture content information from those locations (Lamichhanne 2000) were applied to find matric suction. The results were interpolated to the whole watershed using inverse distance weighted (IDW) methods in GIS. The infiltration depth of probable maximum rainfall for one-day to seven-day cumulative maxima for 25-, 50-, 100-, and 200-year return periods is analyzed.

3.2 Landslide probability

Corominas et al. (2014) indicated that the probability of landslide occurrence in a given area can be obtained using different methods: heuristic (or expert judgment) methods, rational (geomechanical approach) methods, empirical probability, and indirect methods.

Corominas et al. (2014) also suggested an indirect approach to obtain the probability of landside occurrence by relating the frequency of triggering factors, such as earthquakes or rainfall for any watershed. In this research, the indirect approach is applied to estimate landside frequency from the frequency of landslide-triggering rainfall events. A landslide-triggering rainfall event X occurs for precipitation more than the threshold rainfall Xt in a given time period for any watershed. The return period of the threshold rainfall may be defined as the average recurrence interval between events equal to or exceeding the threshold rainfall for this watershed. The probability of any rainfall event more than the threshold rainfall is the product of the probability of a rainfall event less than the threshold rainfall times the probability of one event more or equal to the threshold rainfall. The expectation of recurrence period $E(t)$ can be defined as given below (Chow et al. 1988):

$$E(t) = \sum_{t=1}^{\infty} t(1-p)^{t-1}p \qquad (1)$$

where p is the probability of the event and t is the time period:

$$= p + 2(1-p)p + 3(1-p)^2 p + \cdots$$
$$= p\left[1 + 2(1-p) + 3(1-p)^2 + \cdots\right]$$

$$E(t) = p\left[(1-(1-p))\right]^{-2} \qquad (2)$$

$$E(t) = \frac{p}{\left[1-(1-p)\right]^2} = \frac{1}{p} = T \qquad (3)$$

where the return period T of a rainfall event is the inverse of the probability, as the rainfall event is a random event, independent of space and time.

The probability of a rainfall event X exceeding the threshold rainfall, Xt, for landslide initiation in a watershed can be written as $P(X \geq Xt) = 1/T$. This is an annual probability of the rainfall. The probability of any rainfall greater than the threshold rainfall for a given year period N is

$$= 1 - (1-p)^N, \qquad (4)$$

$$\text{or, the probability of threshold rainfall at least once in } N \text{ year} = 1 - \left(1 - \frac{1}{T}\right)^N. \qquad (5)$$

Landslides do not occur during the maximum rainfall of every year, but may occur when both rainfall duration and intensity increase beyond the threshold value. These rainfall durations and intensities, which trigger landslides, are extreme values in the probability distribution function. These extreme values may appear a couple of times in a single year or not at all in some years. The probability distribution of these events must consider them as extreme value events and therefore requires the application of an extreme value distribution function for probability analysis (Chow et al. 1988).

Extreme value observation lies in the initial or end of the probability distribution function of all observations. Chow et al. (1988) mentioned that there are three ways to analyze these observations based on the location of interest in the distribution function such as high, low, or normal rainfall. These are extreme value distribution type I, type

II, and type III. Extreme rainfall events are mostly modeled by the extreme value type I distribution (Chow et al. 1988; Tomlinson 1980; Chow 1953). The extreme value type I probability distribution function can be written as given below (Chow et al. 1988):

$$F(x) = \exp\left[-\exp\left(-\frac{x-u}{\alpha}\right)\right] \quad -\infty \leq x \leq \infty \tag{6}$$

$$\text{Parameters } \alpha = \frac{\sqrt{6s}}{\pi} \tag{7}$$

$$u = \bar{x} - 0.5772\alpha \tag{8}$$

where u is the mode of distribution (almost at the maximum probability density location), $\bar{x}$ is the average, s is the standard deviation,

$$\text{If } \left(\frac{x-u}{\alpha}\right) \text{ is replaced with } y \tag{9}$$

From Eq. (6.6):

$$y = -\ln\left[\ln\left(\frac{1}{F(x)}\right)\right] \tag{10}$$

For return period T:

$$y_T = -\ln\left[\ln\left(\frac{T}{T-1}\right)\right] \tag{11}$$

From Eq. (6.10):

$$X_T = u + \alpha y_T \tag{12}$$

$$X_T = u + \alpha\left[-\ln\left[\ln\frac{T}{T-1}\right]\right] \tag{13}$$

For a given return period T, the probability of rainfall X_T at least once, other parameters as defined above.

Rainfall data from 1980 to 2013 in the selected gauge station (Chisapani Ghadi) were used in the analysis (Paudel 2018). From these data, one-day to seven-day period cumulative annual maximum rainfall dates were identified. The cumulative rainfall on those dates was developed for each year from 1980 to 2013. Among these data, one-day (24-hour) maximum annual events were modeled using Log Pearson type II and type I. It is found that the extreme values obtained from the frequency analysis are significantly lower in type II than the extreme value of type I distribution. For further frequency analysis, the extreme value of type I is considered. The annual probability of one-day cumulative maximum rainfall to seven-day cumulative maximum rainfall is analyzed. The associated probability of rainfall-induced landslide area is computed. Analysis of the return periods of 25, 50, 100, and 200 years is used for probable rainfall at least once annually. The rainfall event within the given duration from one to seven days, and return period of 25 to 200 years are applied in the landslide initiation analysis.

3.3 Landslide initiation or susceptibility assessment

The identification and mapping of landslide-susceptible zones with threshold rainfall are necessary for hazard assessment. Rainfall-induced landslide susceptibility has been studied by several authors, such as Horton et al. (2013), Park et al. (2013), Tsai and Chiang (2013), Chiang et al. (2012), Enrico and Antonello (2012), Meyer et al. (2012), Kim et al. (2010) Muntohar and Liao (2009), Fall (2009a, b), and Fall et al. 2006. Some of the models used by these researchers required a large number of input data and complex procedures. Besides dealing with a huge data-driven complex relation of rainfall and slope instability, a simple model coupled with rainfall thresholds is a more practical approach for landslide susceptibility assessment (Casadel et al. 2003). Furthermore, the empirical relation of rainfall intensity and duration to landslide initiation can be found in Saito et al. (2010), Zezere et al. (2005), Aleotti (2004), Crosta and Fratini (2001), Ceriani et al. (1994), Wieczorek (1987), and Cancelli and Nova (1985). For mountains in Nepal, Dahal and Hasegawa (2008) recommended a relation of threshold rainfall intensity and duration for landslide initiation. However, their method does not consider influencing factors, such as topography, soil characteristics, and groundwater (Rahardjo et al. 2007). After comparing various models, Chen and Young (2006), Casadel et al. (2003), Hsu et al. (2002), and Claunitzer et al. (1998) suggested a simple rainfall and slope stability model for practical applications. Considering this, the following models are selected for landslide susceptibility assessment.

Slope stability model The slope stability for an unsaturated slope proposed by Fredlund et al. (1987) and Cho and Lee (2002) is considered in this research. This method can consider the initiation of landslide at different rainfall thresholds. The depth of the wetting front Z_w will be equivalent to H in Eq. (14) for the stability analysis.

$$F_s = \left[\frac{\left(\left(c' + (u_a - u_w) \tan \varnothing^b \right) + \left((\sigma_n - u_a) \tan \varnothing' \right) \right)}{(\gamma_t H \sin\beta \cos\beta)} \right] \qquad (14)$$

where F_s = factor of safety (FoS), c' is effective cohesion, $\varnothing'$ is effective friction angle, σ_n is normal stress, H is wetting front depth, β is slope angle, γ_t, is the unit weight of soil, u_a is pore air pressure, u_w is the pore water pressure, $(u_a - u_w)$ is matric suction, $\sigma_n - u_a$ is effective normal stress on the slip surface, e, and $\varnothing^b$ is the rate of increase in shear strength due to matric suction.

The infinite slope stability Eq. (14) has an unsaturated soil suction portion $(u_a - u_w) \tan\varnothing^b$. If the soil degree of saturation reaches 100%, this portion of the soil strength parameter becomes zero and will be similar to saturated conditions. Various models are available for identification of $(u_a - u_w) \tan\varnothing^b$ in terms of $\tan\varnothing'$ (Khalili and Khabbaz 1998; Fredlund et al. 1996; Vanapalli et al. 1996). The equivalent shear strength relation proposed by Fredlund et al. (1996), given in Eq. (15), is used in this study.

$$t_f = c' + (\sigma_n - u_a) \tan \phi' + (u_a - u_w) \left[(\theta^k) \tan \phi' \right] \qquad (15)$$

where t_f is shear strength, Θ is the normalized water content (Θ_w / Θ_s), Θ_w is water content at a given suction, and Θ_s is saturated water content. After Garven and Vanapalli (2006), and Vanapalli and Fredlund (2000), the fitting parameter k is related to the plasticity index (I_p) of soil in % and is given in Eq. (16).

$$k = -0.0016 I_p^2 + 0.0975 I_p^2 + 1 \qquad (16)$$

For non-plastic soil, I_p will be zero and the fitting parameter k is equal to 1, which leads to $\tan\emptyset^b$ equal to $\Theta \tan\emptyset'$.

Unsaturated soil shear strength (Vanapalli et al. 1996; Fredlund et al. 1978) can be obtained from soil–water characteristic curve (SWCC). Empirical relations developed based on grain size distribution by previous researchers, Torres (2011), Fredlund and Xing (1994, Eq. (17)), and Zapata (1999), are applied to obtain the soil water characteristics curve. The modified SWCC model proposed by Fredlund and Xing (1994), Eq. (17), requires various parameters. These parameters are: degree of saturation (S); soil suction at residual moisture content, h_r in kPa; a soil parameter related to the rate of water extraction of the soil after air entry value (a), n (b_f); the slope of the SWCC; m (c_f), which is a fitting parameter or function of the residual water content; air soil parameter, a, which is a function of the air entry value in kPa; soil suction Ψ, in kPa; the initial volumetric water content θ_w; and the volumetric water content in saturated conditions θ_s.

$$S(\%) = \frac{\theta_w}{\theta_s} = 1 - \frac{\ln\left(1 + \frac{\Psi}{h_r}\right)}{\ln\left[1 + \left(\frac{1,000,000}{h_r}\right)\right]} x \left[\frac{1}{\left\{\ln\left[e + \left(\frac{\Psi}{a}\right)^{b_f}\right]\right\}^{c_f}}\right] \tag{17}$$

The empirical model Eq. (18) proposed by Torres (2011) is applied here to obtain SWCCs in which all grain sizes are used in the model. The detail of the analysis method is given in Torres (2011) and implemented in Paudel (2018). The wPI term in Eq. (18) can be obtained from Eq. (19), in which P_{200} is percentage passed through a 200-number of sieve, and PI is the plasticity index.

$$\log \Psi = 0.00005(w\text{PI})^3 - 0.003(w\text{PI})^2 + 0.03w\text{PI} + 1.1355 - (0.0126w\text{PI} + 0.7285)\log D$$
$$- (0.001w\text{PI} + 0.0044)\log D^2 + (0.0002w\text{PI} + 0.0056)\log D^3 \tag{18}$$

$$w\text{PI} = \frac{P_{200}(\text{PI})}{100} \tag{19}$$

where wPI = weighted plasticity index in %, P_{200} = material passing through a #200 US standard sieve in %, PI = plasticity index, expressed in %.

Infiltration model Based on a wetting front concept (Zhang et al. 2011; Chen and Young 2006; Tsai and Yang 2006; Freeze and Cherry 1979; Green and Ampt 1911), Green and Ampt's original Eq. (20) is applied in the analysis for finding the infiltration depth (Z_w) for different threshold rainfall durations T_w. Equation (21) is for the iteration process.

$$T_w = \frac{1}{K_w}\left[Z_w - \psi\Delta\theta \ln\left[\frac{Z_w}{\psi\Delta\theta} + 1\right]\right], \tag{20}$$

or

$$Z_w = Kt + \psi * \Delta\theta \ln\left(1 + \frac{Z_w}{\psi * \Delta\theta}\right) \tag{21}$$

$$\Delta\theta = \theta_1 - \theta_0 \tag{22}$$

where ψ is the suction head at the wetting front in the water column, $\Delta\theta$ is the difference in volumetric water content between the initial and final water content, t is rainfall duration, T_w is rainfall duration equivalent to threshold rainfall, θ_0 is the initial volumetric water content before wetting, θ_1 is the final volumetric water content after wetting, and k is the coefficient of permeability of the soil in the wetted zone.

Tsai and Yang (2006), Chow et al. (1988), and Freeze and Cherry (1979) studied the variation of infiltration capacity of any soil with rainfall intensity and duration. When the infiltration capacity is higher than the rainfall intensity, rainfall intensity governs the infiltration; and if rainfall intensity is greater than the permeability coefficient, infiltration will be governed by permeability. Infiltration depends on soil permeability and initial moisture content. If permeability is in a steady state condition and the soil has no moisture storage, infiltration depends on permeability alone.

The rainfall intensity considered in this analysis is assumed to be evenly distributed within the watershed.

The average soil strength parameters observed in old landslide areas are applied to the entire watershed (Cohesion 11 kPa, Friction 28°). The soil suction applied in the analysis range from 1 to 23 for 73 locations. Unit weight, friction angle, suction, and wetting depth maps are prepared as required for FoS computation in map algebra. These raster maps are used to compute the FoS in the GIS environment. The landslide-susceptible watershed area based on an FoS of less than one for different rainfall is developed. The final landslide susceptibility maps are developed for different rainfall durations and intensities. Landslide susceptibility is classified in three categories: low-susceptibility areas with a FoS greater than two; medium susceptibility with an FoS between one and two; and highly susceptible area with an FoS of less than one. From the highly susceptible areas, landslides initiate and change into debris flows and then travel to the other parts of the watershed. This information is used in the GIS environment for debris flow hazard map development.

3.4 Debris flow runout assessment

Most of the rainfall-induced initial landsides in the study watershed change into destructive debris flows (Dhital 2000). Landslide source area and travel distance covered by debris must be assessed separately, as the extent of these areas depends on different factors (Fell et al. 2008). Various models have been proposed for debris flow runout assessment. These are empirical (e.g., Hurlimann et al. 2008; Hunter and Fell 2003; Legros 2002), semi-empirical, and dynamic models (e.g., Wang et al. 2008; Iverson et al. 1997; Savage and Baum 2005; Sassa and Wang 2005). Debris flow is a complex physical phenomenon and requires detailed information of debris characteristics, terrain topography, in situ moisture conditions, and information about other influencing factors for its runout analysis (Wieczorek and Naeser 2000). The dynamic analysis models require the above information in detail. To obtain a reasonable result from analysis based on limited information, empirical methods present better options (Horton et al. 2013; Carrara et al. 2008; Finlay et al. 1999). In this research, empirical methods are considered for debris flow runout assessment. Previously developed landslide susceptibility maps (Paudel 2018) are considered as debris flow source maps for debris flow analysis. The probable cumulative rainfall for one- to seven-day periods for return periods of 25, 50, 100, and 200 years are used for landslide susceptibility and probability analysis. Later, a landside susceptible area, which has a slope stability FoS of less than one is used as a debris flow source.

Debris flow runout analysis is carried out with various algorithms using the Flow-R software (Horton et al. 2013). The Flow-R model can be used for the identification of landslide susceptibility and debris flow runout (Horton et al. 2013). An application of this software can be found in Paudel (2018). Flow-R is an empirical model developed at the University of Lausanne. The Flow-R model has been applied in various regions of the world with valid and reasonable results (Horton et al. 2013). Also, in the Flow-R model, options for user-defined debris flow sources are available for runout-only simulations. There are various algorithms available in this model; however, the algorithm identified by Paudel (2018) for the study watershed is employed for the debris flow runout analysis. The debris flow source is user-defined in this analysis as the source which is analyzed and discussed in Paudel (2018) and Sect. 3.2.

The Flow-R model models listed in Table 1 are selected for analysis in this research (Paudel 2018). In Table 1, the first column contains a list of source identifications. In this research, the model selected for the source identification and definition of source areas does not make any difference. For spreading algorithms, the Holmgren (1994) or Holmgren modified algorithms (Horton et al. 2013) are both appropriate for use in this watershed. Modified Holmgren (1994) algorithms were developed by Horton et al. (2013) by adding with some height (dh) at a central cell location. The details of these algorithms are available in Horton et al. (2013). In the second sub-column of the second main column, there are two options for initial algorithms: weights and direction memory. Direction memory does not show actual debris flow spreading but any of the default (proportional), Cosinus, and Gamma (2000) algorithms provide appropriate runout results. For the friction loss function and energy loss function, algorithms available are two parameters friction model Perla et al. (1980) and the simplified friction-limited model (SFLM) (Corominas 1996). However, a lower travel angle and lower velocity are sufficient to model debris flow runout.

The algorithm suggested by Holmgren (1994) is given in Eq. (23):

$$p_i^{fd} = \frac{\left(\tan B_i\right)^x}{\sum_{j=1}^8 \left(\tan B_j\right)^x} \forall \left\{ \begin{array}{l} \tan B > 0 \\ x\varepsilon[1; +\infty] \end{array} \right\} \tag{23}$$

where i and j are the flow directions, p_i^{fd} is the susceptibility proportion for i direction, B_i and B_j are the slope angle from the central cell in i and j directions. Exponent x varies from one to infinity. When the value of x is equal to one, it represents the multiple flow and decreases the direction with the increase in its value. In modified Holmgren (Horton et al. 2013), the central cell is raised with some height (dh) at a central location, which can be defined by the user in the Flow-R model.

In a natural terrain, slope direction frequently changes with downslope distance, and a function should be capable of capturing the new direction at a new location. This functional process is defined as the persistence function by Horton et al. (2013). Gamma (2000) and Horton et al. (2013) used the persistence function given in Eq. (24) for change in direction with respect to the previous or initial direction:

$$p_i^p = w_{\alpha(i)} \tag{24}$$

where p_i^p is the flow proportion in direction i, according to the weight and inertia of the flow, $w_{\alpha(i)}$, $\alpha(i)$ is the angle from the previous flow direction. The direction algorithms and persistence algorithms can be written as shown in Eq. (25) (Horton et al. 2013). The combined susceptibility of both functions will be at a maximum value in the original cell with p_o, and it will be distributed in the flow directions i and j.

Table 1 Available algorithms in Flow-R model for debris flow propagation

Source area selection	Spreading algorithms			Energy calculation	
	Direction algorithm	Initial algorithm		Friction loss function	Energy limitation
		Weights	Direction memory		
(Only superior sources (debris flows only), energy base discrimination, complete propagation of all source areas (long))	Holmgren (1994)	Exponent 1 to 50	Default, Cosinus, Gamma (2000)	Travel angle From 0.1° to 50°	Velocity 1–50 mps
	Holmgren (1994) modified	Dh from 0.25 m to 70 exponent 0.1 to 50	Len =005 to 100, Open 090 to 300		

Mps meter per second

$$Pi = \frac{p_i^{fd} p_i^p}{\sum_{j=1}^8 p_j^{fd} p_j^{fd}} p_0 \tag{25}$$

where i and j are the flow directions, p_i is the susceptibility value in direction i, p_i^{fd} the flow proportion according to the flow direction algorithm, p_i^p the flow proportion according to the persistence, and P_o the previously determined susceptibility, which is the total initial value or value of the central cell.

In the Flow-R model, the flow mass is considered to be a unit value, and energy loss results entirely from friction. The energy required to travel to another cell must be sufficient for flow to take place from one cell to another. Energy is the controlling factor for runout and spreading to adjacent cells based on the available energy, and the required energy is different between two cells or adjacent cells. The energy required value between cells can be defined by the user. Equation (26) shows this relation (Horton et al. 2013).

$$E_{\text{kin}}^i = E_{\text{kin}}^0 + \Delta E_{\text{pot}}^i - E_{\text{f}}^i, \tag{26}$$

where E_{kin}^i is the kinetic energy of the cell in direction i, E_{kin}^o is the kinetic energy of the central cell, ΔE_{pot}^i is the change in potential energy to the cell in direction i, and E_{f}^i is the energy lost in friction to the cell in direction i.

The simplified friction-limited model (SFLM) suggested by Corominas (1996), and known as Default in the software, is given in Eq. (27):

$$E_i^i = g\Delta x \tan\phi \tag{27}$$

where E_i^f is the energy lost function from the central cell to the cell in i direction, Δx, the horizontal displacement increments in direction i, $\tan\emptyset$, the energy gradient in the direction of i, and g, the acceleration due to gravity.

Horton et al. (2013) developed Eq. (28) for a limiting velocity from a given value. The maximum velocity can be introduced to cap the velocity on the steep slopes and limit the propagation:

$$V_i = \min\left\{ \sqrt{(V_0^2 + 2g\Delta h - 2g\Delta x \tan\phi)},\ V_{\max} \right\} \tag{28}$$

where Δh is the difference in elevation between the central cell and the cell in direction i, and $V_{\max}$ is the given velocity limit. This limit can be defined based on region by the user. The general value of V_i is always limited to $V_{\max}$, and the intermediate value from the first part of Eq. (28).

3.5 Debris flow hazard assessment

The final stage of this study is the debris flow hazard area mapping for the study watershed. When all information is derived and analyzed using the above-mentioned methodology and work steps, these results are applied in the final model as shown in Fig. 2 to create debris flow hazard maps. In this model, landslide-susceptible maps developed using the methodology mentioned in the previous section and a given probability are categorized in three areas. These are: FoS less than one, one to two and more than two in the stability analysis. The watershed areas associated with FoS of less than one in the slope stability analysis are considered to be landslide-susceptible regions. These unstable areas are considered

for debris flow runout analysis and developed debris flow inundation maps. Debris flow inundation areas in the study watershed maps are converted into polygons and included in landslide-susceptible regions, called a debris flow zone, for a given probability. An FoS of one to two is defined as a medium landslide susceptibility zone. The area which has an FoS of more than two is considered a low landslide susceptibility zone for a given probability. Finally, the debris flow zone includes debris flow initiation, inundation, and a buffer of 10 m outlines of these areas.

These debris flow areas are associated directly with the probability of rainfall (annual frequency of return rainfall) in the watershed. The debris flow area, medium-susceptibility, and low-susceptibility zones are analyzed for different return periods. The rainfall return periods used in this study are 25, 50, 100, and 200 years, and rainfall durations cover one-day to seven-day periods. The duration selected is based on conversations with the local elderly people who have extensive experience with rainfall-induced landslide events. Seven-day rainfall has a mythical status in Nepal in relation to landslides. People become scared if rainfall continues up to seven days with considerable intensity, because they believe that a landslide in their area is imminent if such rainfall occurs at any time of the year. However, such events occur mostly between late April and late November. In another study, continuous and longer rainfall caused more landslides in these mountains (Dahal and Hasegawa 2008). The annual probability of the hazard area is analyzed, and the trend of highly hazardous areas and their probability or return period are derived.

4 Debris flow hazard in the study watershed

4.1 Landslide susceptibility maps

The data for landslide-triggering factors in the watershed are applied in Eq. (14) to identify landslide-susceptible areas, as discussed in Sect. 3. Rainfall probability is derived for the probability of landslide-susceptible locations. The rainfall data of the study area are available from 1980 to 2013 and are recorded once every day. The maximum one-day to seven-day rainfall in every year from 1980 to 2013 period is identified and shown in Fig. 4. From Fig. 4, the cumulative rainfall data for one-day maximum, two-day maximum and so on up to seven days may not concede each other. However, most of these maximum rainfall event days are on similar dates (Fig. 4). Figure 4 also shows the cumulative one-day rainfall of 443 mm, and seven-day rainfall of 1033 mm. The rainfall amount of 1033 mm is almost half of the average annual rainfall in the watershed. Within the study period 1980 to 2013, up to half of the annual precipitation can occur in one seven-day event.

These maximum cumulative rainfall amounts are used for annual probability and recurrence period analysis. The return periods chosen for analysis are from 1.01 year to 200 years. Figure 5 shows the probability and return period of rainfall for events of one- to seven-day duration.

From Fig. 5 a higher return period or lower annual probability is linked to more cumulative rainfall. The probability of one-day and seven-day events remains the same, as it is a cumulative maximum taken from each year from 1980 to 2013. The rainfall for a return period of 200 years and an annual probability of 0.005 for one-day duration is 458.39 mm, while for seven days it is 1,051 mm. Similarly, for a return period of 500 years and a probability 0.002, one-day rainfall is 519 mm, and seven-day rainfall 1185 mm. Higher-intensity and longer-duration rainfall are triggering factors for landslide initiation. The duration of
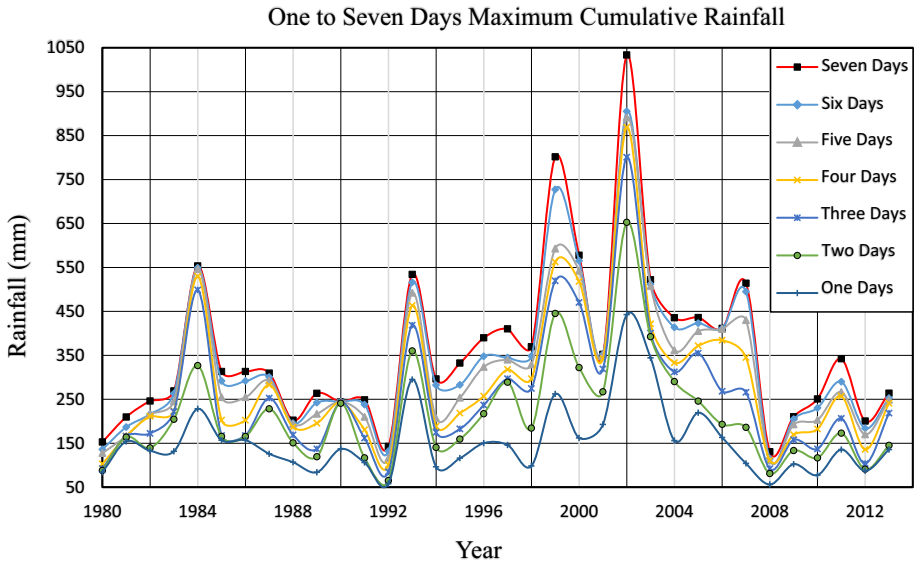
Fig. 4 One- to seven-day maximum cumulative rainfall
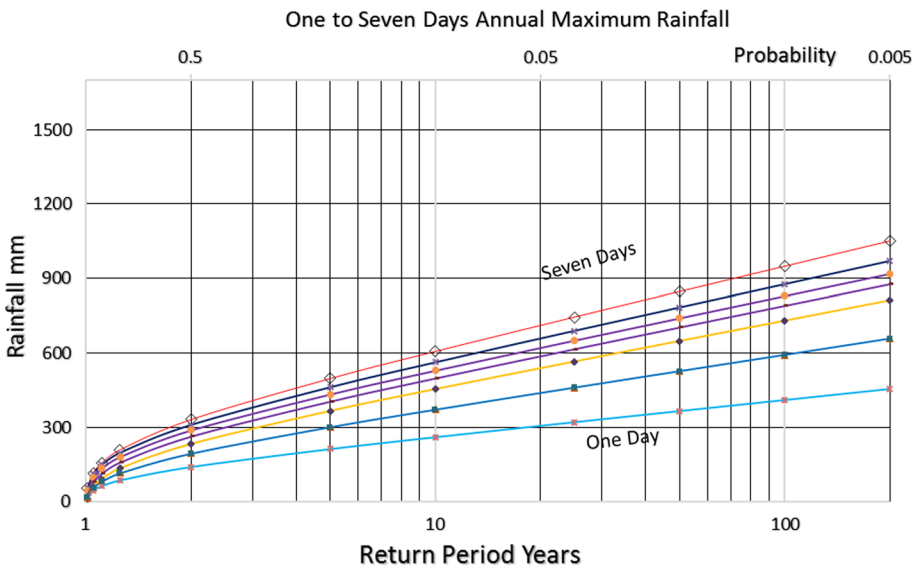

Fig. 5 One-day to seven-day annual maximum rainfall probability and return period

one to seven days and expected rainfall from probability analyses are applied for hazard assessment of the area.

The annual probability of rainfall is computed for up to a 200-year return period. The further analysis of landslide susceptibility is carried out for selected rainfall return periods—once in 25, 50, 100, and 200 years—to obtain a trend of hazard in the watershed

Table 2 Annual rainfall probability and return period for one- to four-day rainfall

Annual rainfall probability	Return period	One-day rainfall		Two-day rainfall		Three-day rainfall		Four-day rainfall	
P	Year	mm	In (cm/sec)	mm	In (cm/sec)	mm	In (cm/sec)	mm	In (cm/sec)
0.04	25	320	0.00037	460	0.00027	565	0.00022	614	0.00018
0.02	50	367	0.00042	526	0.00030	647	0.00025	702	0.00020
0.01	100	413	0.00048	591	0.00034	729	0.00028	789	0.00023
0.005	200	458	0.00053	657	0.00038	811	0.00031	875	0.00025

P probability, *In* infiltration

Table 3 Continued annual rainfall probability and return period for five-, six-, and seven-day rainfall

Annual rainfall probability	Return period	Five-day rainfall		Six-day rainfall		Seven-day rainfall	
P	Year	mm	In (cm/sec)	mm	In (cm/sec)	mm	In (cm/sec)
0.04	25	651	0.00015	689	0.00027	744	0.00015
0.02	50	741	0.00017	783	0.00030	847	0.00017
0.01	100	830	0.00019	877	0.00034	949	0.00019
0.005	200	919	0.00021	970	0.00038	1051	0.00021

P probability, *In* infiltration

rather than all analyses. The expected rainfall for these probabilities and return periods is given in Tables 2 and 3. Also given in these tables is infiltration rate, which is equivalent to rainfall intensity over the period of one to seven days. These infiltration rates and durations of expected rainfall (such as one-day to seven-day) are used for infiltration computations. Landslide susceptibility is computed as in Eq. (14). The location and areas identified as unstable for different rainfall return periods are shown in Figs. 6 and 7. Figure 6a–c shows an annual probability of 0.04 for landslide susceptibility for continuous rainfall over one-, four-, and seven-day periods, while Fig. 6d–f shows a probability of 0.02 for the same duration one-, two-, and seven-day rainfall. Similarly, Fig. 7a–c shows an annual landslide susceptibility probability of 0.01 for one-, four-, and seven-day rainfall period, and Fig. 7d–f shows a probability of 0.005 for one-, two-, four-, and seven-day rainfall periods. The area of landslide susceptibility increases with the higher return period rainfall and number of days' duration.

The summary of the analysis above is shown in Fig. 8. The landslide-susceptible area does not change much for up to a two-day period of rain, but it increases with duration rapidly after that. The rainfall events with low annual probability are linked to a higher landslide-susceptible area. The watershed is 124 km^2 and unstable areas are up to 400 hectares for seven-day rainfall, with a probability of 0.005. The recurrence period of this event is 200 years, and the landslide-susceptible area is 3.25%. The lower the annual probability of rainfall or extreme event, the higher the rainfall intensity and the unstable areas (Table 4).
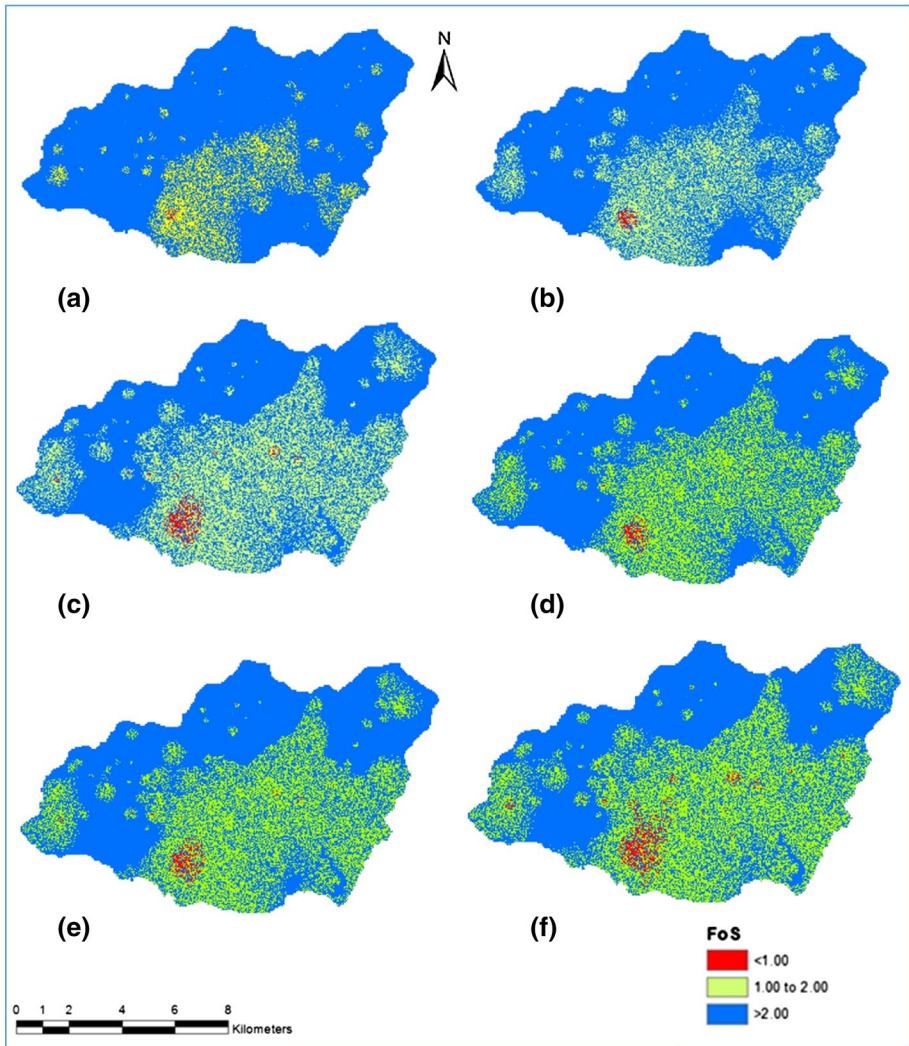
Fig. 6 Landslide susceptibility area for 25-year return period, **a** one-day rainfall, **b** four-day rainfall, and **c** seven-day rainfall; and landslide susceptibility area for 50-year return period, **d** one-day rainfall, **e** four-day rainfall, **f** seven-day rainfall

4.2 Debris flow inundation with susceptibility maps

The landslide susceptibility maps discussed in the previous section are considered to be debris source maps for runout distance analysis. The total landslide initiation areas and debris flow runout areas are merged. These areas are converted into polygons. The total identified unstable and runout debris flow area must have some setback distance. The setback distance depends on the location of the area, physical features, type of development, existing terrain slope, type of slope, and length of slope. Obtaining these features is beyond the scope of this research. Therefore, a constant value of 10 m outer setback distance is
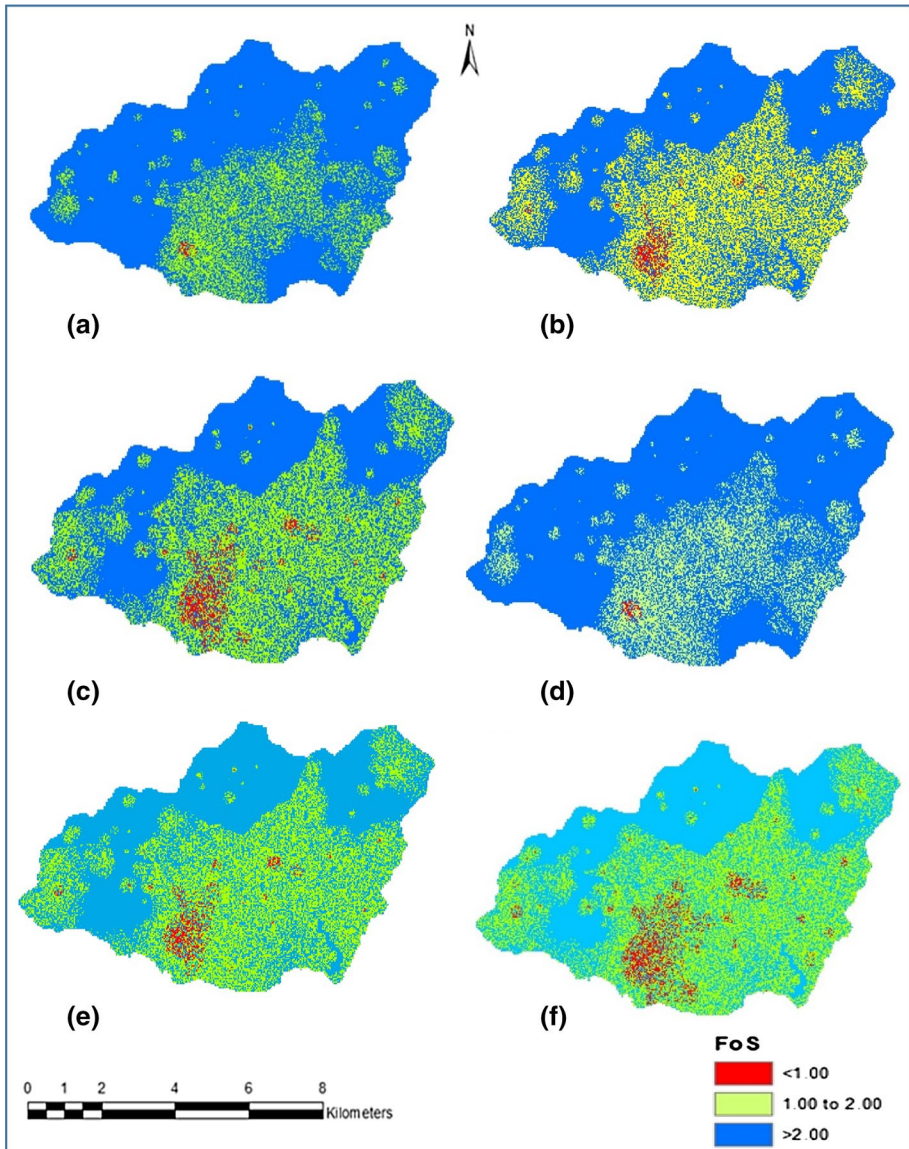
Fig. 7 Landslide susceptibility area for 100-year return period, **a** one-day rainfall, **b** four-day rainfall, and **c** seven-day rainfall; and landslide susceptibility area for 200-year return period, **d** one-day rainfall, **e** four-day rainfall, and **f** seven-day rainfall

used. These polygons are enclosed with a 10-m buffer around the outer area as a setback distance. The final results of this analysis are shown in Fig. 9. Figure 9a–d shows the landslide and debris flow susceptibility area, with a buffer of 10 m, for continuous rainfall over one day with annual probabilities of 0.04, 0.02, 0.01, and 0.005, respectively. Figure 9e–h shows a similar susceptibility area, buffer, and annual probability, but for seven-day continuous rainfall.
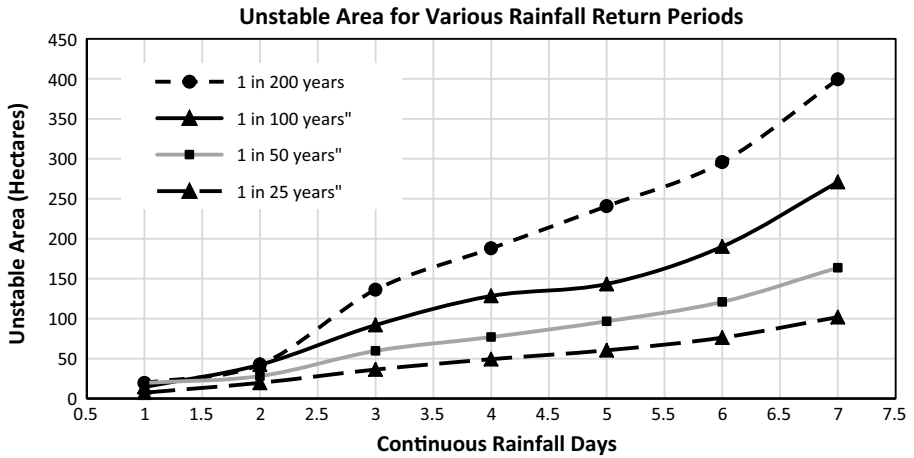
(a) Landslide-susceptible area in hectares
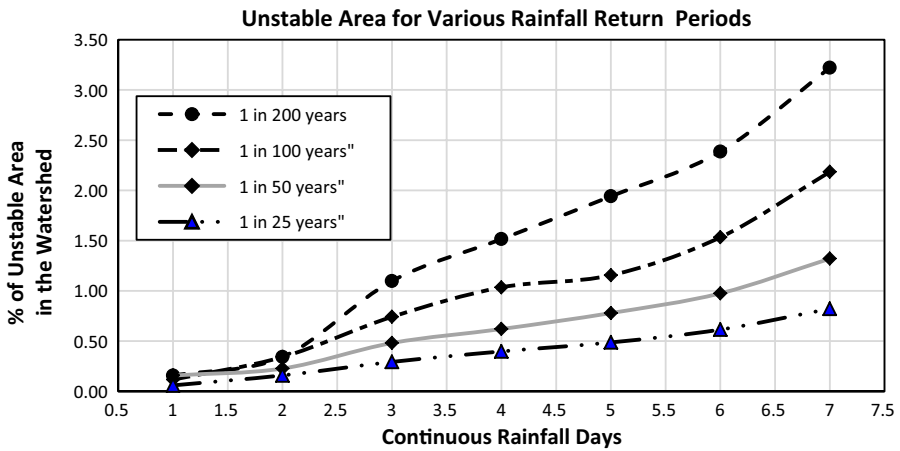
(b) Landslide-susceptible area in percent

Fig. 8 Landslide-susceptible area of the watershed for different return periods and rainfall durations: **a** in hectares; **b** in percent

4.3 Debris flow hazard maps

Debris flow hazard maps are developed by combining landslide initiation and debris flow runout areas. The (probable) debris flow area has an FoS of less than one in the initial slope, debris flow susceptible area, and their buffer of 10 m outlines. The watershed area beyond the debris flow area is also categorized as medium and low landslide susceptibility areas based on the FoS of the stability of the initial slope. The watershed area which has an FoS of one to two is considered to be a medium-(landslide) susceptibility area, and that with more than two as low-susceptibility. The medium-susceptibility area is the map area for FoS of less than two, minus debris flow areas. The low-susceptibility zone has an FoS of more than two, minus the debris flow area and the medium-susceptibility areas. This analysis is carried out for seven-day rainfall and one-day rainfall only and is summarized

Table 4 Hazard area with probability and return period

Return period (years)	Annual probability	Days of rainfall	Total water-shed area (Ha)	Hazard area (Ha)	Medium-suscepti-bility area (Ha)	Low-suscepti-bility area (Ha)
25	0.04	1	12,400	13	1387	11,001
50	0.02	1	12,400	18	2624	9740
100	0.01	1	12,400	24	4998	7802
200	0.005	1	12,400	36	5009	7355
25	0.04	7	12,400	77	3960	8364
50	0.02	7	12,400	154	4365	8035
100	0.01	7	12,400	284	4706	7409
200	0.005	7	12,400	418	8403	7384

in Table 4. The hazard area in the watershed for one-day and 25-, 50-, 100-, and 200-year return rainfall is shown in Fig. 10. Figure 11 shows seven-day rainfall and return periods of 25, 50, 100, and 200 years.

5 Results and discussions

The relation of hazard and susceptibility area to its annual probability for one-day rainfall is shown in Fig. 12. The large high-hazard area is associated with low-probability events, and the low-hazard area with high-probability events, which means that short rainfall return periods are associated with small hazard areas. For seven-day rainfall duration, this relation is shown in Fig. 13. The relation of high hazard areas to their annual probability of occurrence is given in Eqs. (28) and (29). The regression coefficients (R) for Eqs. (29) and (30) are 1.00 and 0.99, respectively.

$$H_1 = 2.7185 P_1^{-0.482} \tag{29}$$

$$H_7 = 5.8841 P_7^{-0.82} \tag{30}$$

where H_1 and H_7 are hazard areas and P_1 and P_7 are the annual probability of occurrence in one-day and seven-day rainfall.

The relation between high hazard area and rainfall return period is derived for a rainfall duration of one day and shown in Fig. 13. A high hazard area as small as 13 ha is observed for 25-year return period rainfall for one-day duration, and up to 77 hectares for seven days. Equations (31) and (32) are the relationships of high hazard with return period for this watershed. The R values for these equations are 1 and 0.997 for one-day and seven-day rainfall periods, respectively.

$$H_{1D} = -0.0081 (RP^2) + 3.771 (RP) + 13 \tag{31}$$

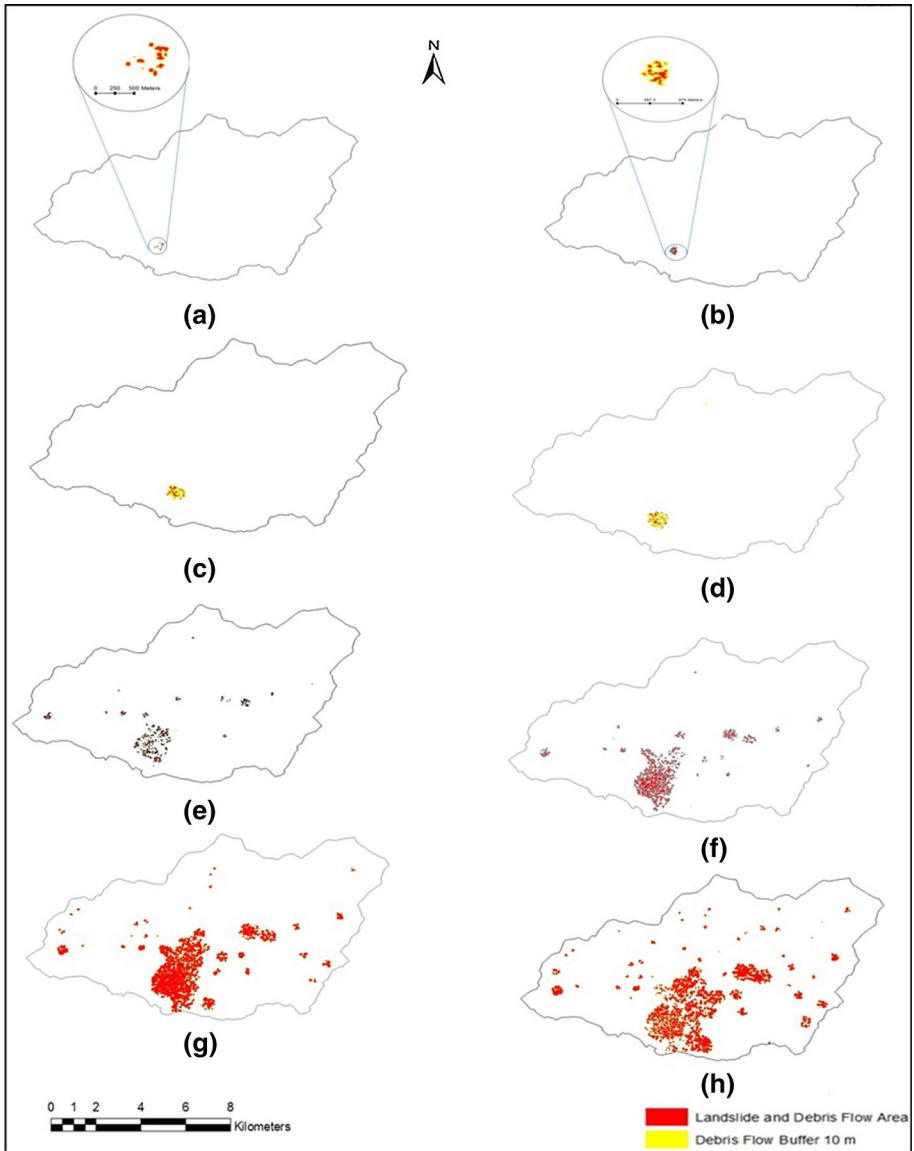$$H_{7D} = -0.0002 (RP^2) + 0.1675 (RP) + 9.33 \tag{32}$$

Fig. 9 Landslide initiation and debris flow susceptible area and buffer areas for one-day rainfall with return periods of **a** 25 years, **b** 50 years, **c** 100 years, and **d** 200 years; and seven-day rainfall with return periods of **e** 25 years, **f** 50 years, **g** 100 years, and **h** 200 years
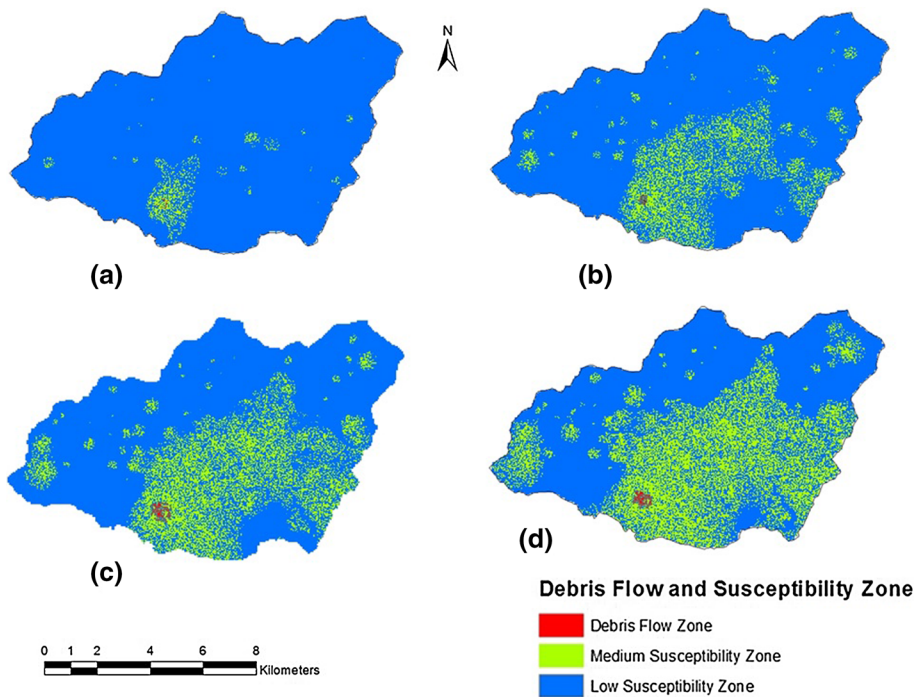
Fig. 10 Debris flow hazard map with 10-m buffer for one-day rainfall with return periods of **a** 25 years ($P=0.04$), **b** 50 years ($P=0.02$), **c** 100 years ($P=0.01$), **d** 200 years ($P=0.005$). P: annual probability

where H_{1D} and H_{7D} are high hazards for one- and seven-day periods and RP is the return period.

6 Summary and conclusions

Recorded rainfall and physical changes are modeled to predict instability in mountain slopes in the study watershed. Annual rainfall probability or respective return periods are applied for rainfall-induced landslide probability assessment. Rainfall records for 34 years (from 1980 to 2013) are available to identify annual one-day to seven-day maximum rainfall. Information regarding the maximum annual cumulative rainfall of the 34-year period is used to calculate annual rainfall probability and return periods. One-day and seven-day maximum cumulative rainfall from the analysis is 443 and 1033 mm, respectively. The annual probability of rainfall computed for 1.01 to 200-year return periods has annual probabilities of 0.990,099 to 0.005. The rainfall for a return period of 200 years and an annual probability of 0.005 for one-day duration is 458 mm, while for seven days it is 1051 mm. The infiltration rate is identified from the rainfall intensity duration of the selected annual probability. For the landslide susceptibility analysis, only four return periods 25, 50, 100, and 200 years (annual probability 0.04 to 0.005) are selected to find a trend of landslide susceptibility with annual probability or return period in the watershed.
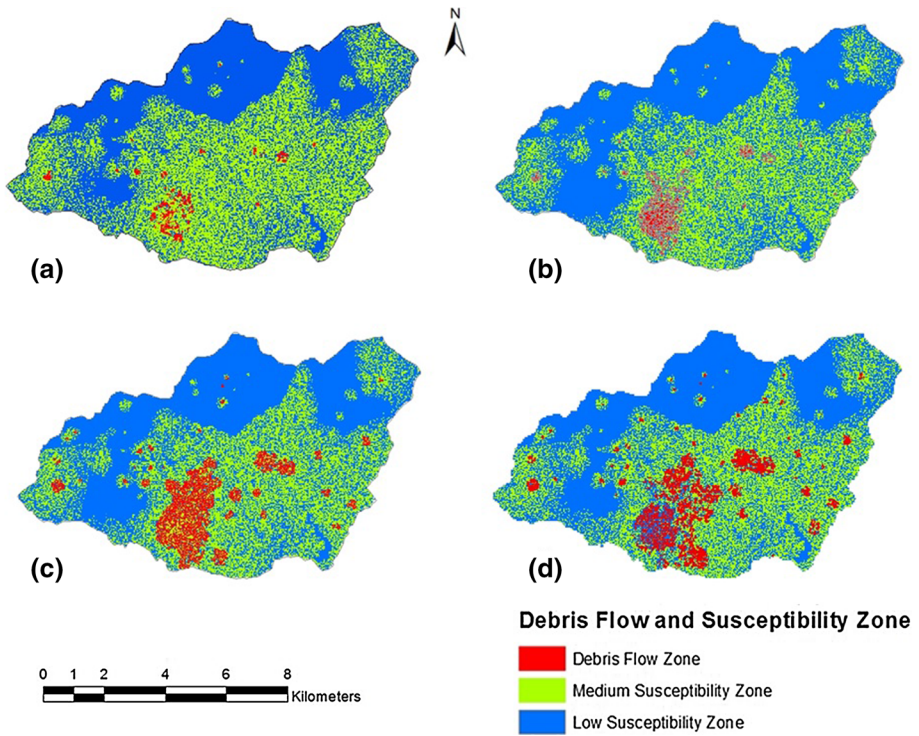
Fig. 11 Landslide hazard map with a 10-m buffer for seven-day rainfall with return periods of **a** 25 years ($P=0.04$), **b** 50 years ($P=0.02$), **c** 100 years ($P=0.01$), **d** 200 years ($P=0.005$). *P*: annual probability
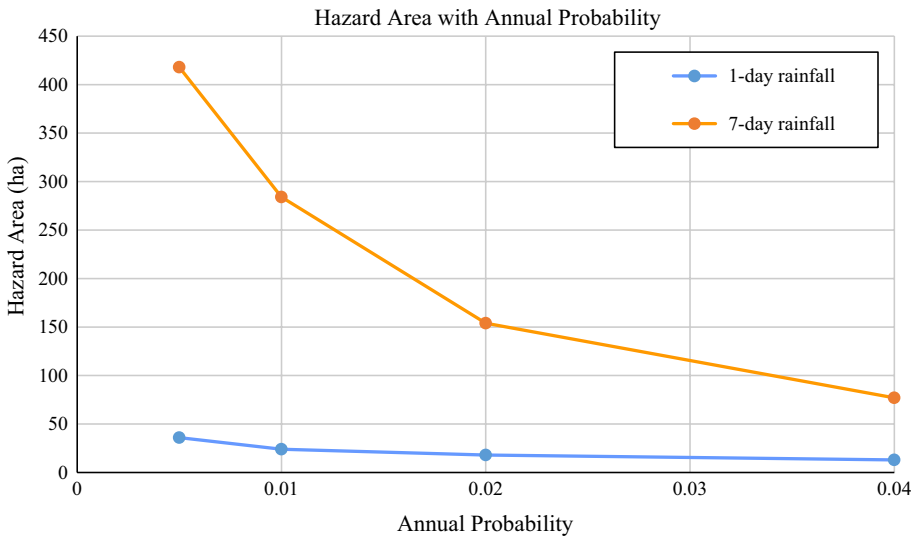

Fig. 12 Landslide hazard area with 10-m buffer for annual probability for one-day and seven-day rainfall
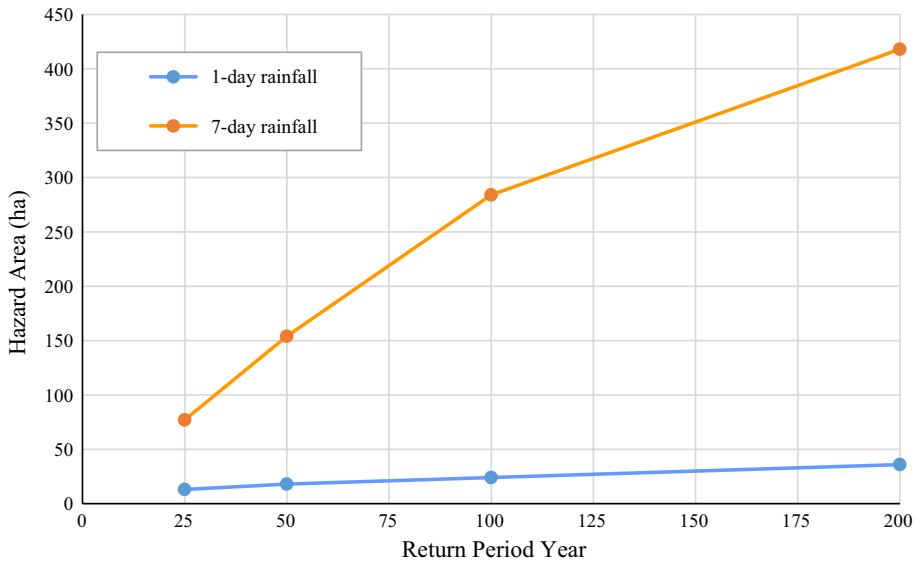
Fig. 13 Landslide hazard area and return period with 10-m buffer for one-day and seven-day rainfall

Data from a geotechnical investigation conducted in one recent landslide location within the study area are considered for stability analysis. SWCC is developed using a grain size distribution model from soil samples received from 73 locations (Lamichhanne 2000) in the watershed. The grain size distribution model is used for matric suction with respect to the in situ moisture content of these locations. The landslide-susceptible locations and area of the watershed with a given probability is identified. The landside susceptibility is analyzed for one-, four-, and seven-day periods and the return periods mentioned above. The area of landslide susceptibility increases with the higher return period rainfall and number of days.

Susceptibility areas are categorized as high, medium, or low-susceptibility based on an FoS of less than one, one to two, and more than two, respectively. The watershed area is 124 km^2, and the unstable portion is up to 400 hectares for seven-day rainfall with an annual probability of 0.005. The recurrence period of this event is 200 years. The landslide-susceptible area is 3.25% of the total watershed area. The longer-duration and higher-intensity rainfall are trigger factors for rainfall-induced landslides.

The hazard zone (FoS less than one) of the watershed is considered as a source of landslides for debris flow analysis. The Flow-R model is applied for debris flow runout and inundation area computation. In the Flow-R model, susceptible areas developed from slope stability analysis are considered as a user-defined debris flow source. The Holmgren (1994) modified algorithm is used for debris flow spreading. For the initial algorithm, Weights was chosen. The Weights algorithms have three sub-algorithms: the default algorithm, Gamma (2000), and Cosinus. Any of these algorithms provides appropriate debris flow spreading in this region; however, the default is chosen for the analysis, which is a proportional method of spreading to adjacent cells. Friction loss function and energy limitation algorithms are available and used in the energy calculation. The low travel angle and low velocity were appropriate for debris flow runout analysis for this watershed, and these are chosen for friction loss function and energy limitation.

The debris flow area and landslide initiation area from the susceptibility analysis are combined in a single map to develop hazard maps. These combined total areas are transformed into polygons. The landslide hazard area required a setback distance which depends on various factors, including type of soil, proximity of river or water body, and topography. Individual polygon setback distance analysis is beyond the scope of this research, and therefore, a 10-m setback distance is chosen for all polygons and buffers them from the outer side. The final area within the buffered mark is termed the hazard area. For return periods of 25, 50, 100, and 200 years, one-day and seven-day duration rainfall intensity are used for these analyses. For the 25-year return period and one-day duration rainfall, the computed hazard area is 13 hectares (ha), while for the 200-year return period it is 36 ha. This area drastically changed for seven-day rainfall as it is 77 ha for a 25-year return period and 418 ha for a 200-year return period. Large return periods with high duration rainfall are hazardous in the study watershed.

The landslide hazard areas for different return periods are developed for the study watershed. The annual rainfall probability (recurrence period) and hazard location in any watershed is important for policy makers. For instance, if an area is hazardous for a 1 in 25 year event, it should be avoided for hospitals, school buildings, or any such community facility services. It may or may not be suitable for residential development depending on other factors and the decision of the local authority.

This study is a part of landslide risk assessment modeling for the watershed scale. The hazard is assessed using unsaturated soil technology and rainfall effects on sloping ground. Methods used for analysis are open-source computing tools for hazard assessment. The method can be used for developing landslide hazard risk and as support for making land use plans in similar hazardous areas. This study provides an indirect probability assessment for potential rainfall-induced landslide locations within the watershed. The areas of landslide susceptibility, debris flow inundation, and setback distance are considered as a landslide hazard area within the study area for a given time and location. Based on government policies for any watershed or location, these methods can be applied to estimate the risk of any development in any proposed area before planning these activities. This will reduce physical, societal, environmental, and economic hazard in the study watershed. Hazard return periods and the design life of a proposed development plan or structure can be compared before implementing their construction in the area.

References

Aleotti P (2004) A warning system for rainfall-induced shallow failures. Eng Geol 73:247–265

Cancelli A, Nova R (1985) Landslides in soil debris cover triggered by rainstorms in Valtellina (central Alps–Italy). In: Proceedings of the 4th international conference and field workshop on landslides, The Japan Geological Society, Tokyo, pp 267–272

Carrara A, Crosta G, Frattini P (2008) Comparing models of debris-flow susceptibility in the alpine environment. Geomorphology 94:353–378

Casadel M, Dietrich WE, Miller NL (2003) Testing a model for predicting the timing and location of shallow landslide initiation in soil-mantled landscapes. Earth Surf Process Landf 28:925–950

Ceriani M, Lauzi S, Padovan N (1994) Rainfall thresholds triggering debris-flows in the alpine area of Lombardia Region, central Alps–Italy. In: Proceedings of man and mountain, I conference international per laProtezione e lo Sviluppo dell'ambiente montano, Ponte di legno (BS), pp 123–139

Chen L, Young MH (2006) Green-Ampt infiltration model for sloping surfaces. Water Resour Res 42:W07420. https://doi.org/10.1029/2005WR004468

Chiang SH, Chang KT, Mondini AC, Tsai BW, Chen CY (2012) Simulation of event-based landslides and debris flows at watershed level. Geomorphology 138:306–618

Cho SE, Lee SR (2002) Evaluation of surficial stability for homogeneous slopes considering rainfall characteristics. J Geotech Geoenviron Eng 128(9):756–763

Chow VT (1953) Frequency analysis of hydrologic data with special application to rainfall intensities bulletin no 414 University of Illinois, Engineering Experiment Station

Chow VT, Maidment DR, Mays LW (1988) Applied Hydrology. McGraw Hill Book Company, New York. ISBN 0-07-010810-2

Claunitzer V, Hopmans JW, Starr JL (1998) Parameter uncertainty analysis of common infiltration models. Soil Science Soc Am J 62:1477–1487

Corominas J (1996) The angle of reach as a mobility index for small and large landslides. Can Geotech J 33:260–271

Corominas J, Van Westen C, Frattini P, Cascini L, Malet J-P, Fotopoulou S, Catani F, Van Den Eeckhaut M, Mavrouli O, Agliardi F, Pitilakis K, Winter MG, Pastor M, Ferlisi S, Tofani V, Hervas J, Smith JT (2014) Recommendations for the quantitative analysis of landslide risk. Bull Eng Geol Environ 73:209–263

Crosta GB, Frattini P (2001), Rainfall thresholds for triggering soil slips and debris flow. In: Mugnai A, Guzzetti F, Roth G (eds) Proceedings of the 2nd EGS Plinius conference on Mediterranean storms, Siena, Italy, pp 463–487

Dahal RK, Hasegawa S (2008) Representative rainfall thresholds for landslides in the Nepal Himalaya. Geomorphology 100(3-4):429–443

Deoja BB, Dhital MR, Thapa B, Wagner A (1991) Mountain risk engineering handbook, International Centre for Integrated Mountain Development (ICIMOD), Kathmandu, Nepal, p 875

Dhakal AS, Amada T, Aniya M (2000) landslide hazard mapping and its evaluation using GIS: an investigation of sampling scheme for grid-cell based quantitative method. Photogramm Eng Remote Sens 66:981–989

Dhital MR (2000) An overview of landslide hazard mapping and rating systems in Nepal. J Nepal Geol Soc 22:533–538

Dhital MR (2003) Causes and consequences of the 1993, debris flows and landslides in the Kulekhani watershed, central Nepal. In: Rickenmann and Chen (eds) Debris-flow hazards mitigation: mechanics, prediction and assessment, pp 1931–1943

DWIDP, Department of Water Induced Disaster Prevention (2017) Annual disaster review 2009. Report, Ministry of Irrigation, Government of Nepal, Kathmandu, pp 208

Enrico C, Antonello T (2012) Simplified approach for the analysis of rainfall-induced shallow landslides. J Geotech Geoenviron Eng 138:398–406

Fall M (2009a) A GIS-based mapping of historical coastal cliff recession. Bull Eng Geol Environ 68(4):473–482

Fall M (2009b) Lecture notes hazard assessment. University of Ottawa, Ottawa

Fall M, Azzam R, Noubactep C (2006) A multi-method approach to study the stability of natural slopes and landslide susceptibility mapping. Eng Geol 82(2006):241–263

Fell R, Corominas J, Bonnard CH, Cascini L, Leroi E, Savage WZ (2008) Guidelines for landslide susceptibility, hazard and risk zoning for land use planning. Eng Geol 102:85–98

Finlay PJ, Mostyn GR, Fell R (1999) Landslide risk assessment prediction of travel distance. Can Geot J 36:556–562

Fredlund DG, Xing AE (1994) Equation for the soil-water characteristic curve. Can Geotech J 31:521–532

Fredlund DG, Morgenstern NR, Widger RA (1978) Shear strength of unsaturated soils. Can Geotech J 15:313–321

Fredlund DG, Rahardjo H, Can JKM (1987) Nonlinearity of strength envelope for unsaturated soils. In: Proceedings of the 6th international conference on expansive soils, New Delhi, India, pp 49–54

Fredlund DG, Xing A, Fredlund MD, Barbour SL (1996) The relation of the unsaturated soil shear strength to the soil-water characteristics curve. Can Geotech J 33:440–448

Freeze A, Cherry JA (1979) Groundwater. Prentice Hall Inc, Englewood Cliffs

Gamma P (2000) dfwalk—Ein Murgang-Simulationsprogramm zur Gefahrenzonierung, Geographisches Institut der Universität Bern. (**in German**)

Garven E, Vanapalli SK (2006) Evaluation of empirical procedures for predicting the shear strength of unsaturated soils. American Society of Civil Engineers Geotechnical Special Publication No. 147, vol 2, pp 2570–2581

Green WH, Ampt CA (1911) Studies on soil physics: flow of air and water through soils. J Agric Sci 4:1–24

Guzzetti F (2005) Landslide hazard and risk assessment, Ph.D. Dissertation Rheinischen Friedrich-Wilhelms Univestitat Bonn

Guzzetti F, Carrara A, Cardinali M, Reichenbach P (1999) Landslide hazard evaluation: an aid to a sustainable development. Geomorphology 31:181–216

Holmgren P (1994) Multiple flow direction algorithms for runoff modelling in grid based elevation models: an empirical evaluation. Hydrol Process 8:327–334

Horton P, Jaboyedoff M, Rudaz B, Zimmermann M (2013) Flow-R, a model for susceptibility mapping of debris flows and other gravitational hazards at a regional scale. Nat Hazards Earth Syst Sci 13:869–885

Hsu SM, Ni CF, Hung PE (2002) Assessment of three infiltration formulas based on model fitting on Richard's equation. J Hydrol Eng 7(5):373–379

Hunter G, Fell R (2003) Travel distance angle for 'rapid' landslides in constructed and natural soil slopes. Can Geotech J 40(6):1123–1141

Hurlimann M, Rickenmann D, Medina V, Medina V, Beteman A (2008) Evaluation of approach to calculate debris-flow parameters for hazard assessment. Eng Geol 102:152–163

Iverson RM, Reid ME, La Husen RG (1997) Debris flow mobilization from landslides. Annu Rev Earth Planet Sci 25:85–138

Jaiswal P, Van Westen CJ, Jetten V (2011) Quantitative estimation of landslide risk from rapid debris slides on natural slopes in the Nilgiri hills, India. Nat Hazards Earth Syst Sci 11:1723–1743

Kayastha P, Dhital MR, Smedt FD (2013) Evaluation and comparison of GIS based landslide susceptibility mapping procedures in Kulekhani watershed, Nepal. J Gelo Soc India 81:219–231

Khallili N, Khabbaz MH (1998) A unique relationship for the determination of the shear strength of unsaturated soils. Geotechnique 48(5):681–687

Kim D, Im S, Lee SH, Hong Y, Cha KS (2010) Predicting the rainfall-triggered landslides in a forested mountain region using TRIGRS model. J Mt Sci 7:83–91

Lamichhanne SP (2000), Engineering geological watershed management studies in the Kulekhani watershed, M.Sc. thesis, Tribhuvan, University, Nepal

Legros F (2002) The mobility of long-runout landslide. Eng Geol 63:301–331

Meyer NK, Dyrrdal AV, Frauenfelder R, Etzelmuller B, Nadim F (2012) Hydrometeorological threshold conditions for debris flow initiation in Norway. Nat Hazards Earth Syst Sci 12:3059–3073

Ministry of Home (2011, 2012, 2013, 2015, 2016), Disaster Report (http://neoc.gov.np/en/)

Ministry of Home, Nepal Disaster Report (2015) public web resource: http://neoc.gov.np/en/publication/

Muntohar AS, Liao HJ (2009) Analysis of rainfall-induced infinite slope failure during typhoon using a hydrological–geotechnical model. Environ Geol 56:1145–1159

Park DW, Nikhil NV, Lee SR (2013) Landslide and debris flow susceptibility zonation using TRIGRS for the 2011 Seoul landslide. Nat Hazards Earth Syst Sci 13:2833–2849

Paudel B (2018) GIS-based assessment of debris flow susceptibility and hazard in mountainous regions of Nepal. Ph.D. dissertation, University of Ottawa, Canada, p 232

Perla R, Cheng TT, McClung DM (1980) A two-parameter model of snow-avalanche motion. J Glaciol 26:197–207

Rahardjo H, Ong TH, Rezaur RB, Leong EC (2007) Factors controlling instability of homogeneous soil slopes under rainfall. J Geotech Geoenviron Eng 133(12):1532–1543

Reid LM, Page MJ (2003) Magnitude and frequency of landsliding in a large New Zealand catchment. Geomorphology 49(1–2):71–88

Remondo J, Bonachea J, Cendrero A (2008) A statistical approach to landslide risk modelling at basin scale; from landslide sus-ceptibility to quantitative risk assessment. Geomorphology 94(2008):496–507

Saito H, Nakayama D, Matsuyama H (2010) Relationship between the initiation of a shallow landslide and rainfall intensity duration thresholds in Japan. Geomorphology 118:167–175

Sassa K, Wang G (2005) Mechanism of landslide-triggered debris flows: liquefaction phenomena due to the undrained loading of torrent deposits. Debris-flow Hazards and Related Phenomena. Praxis Publishing Ltd, Chichester, pp 81–104

Savage W, Baum R (2005) Instability of steep slopes. Debris-flow hazards and related phenomena. Praxis Publishing Ltd, Chichester, pp 53–79

Tomlinson AI (1980) The frequency of high intensity rainfall in New Zealand, Water and Soil Tech. Publ. no 19, Ministry of Work and Development, Wellington, New Zealand

Torres GH (2011) Estimating the soil-water characteristics curve using grain-size analysis and plasticity index, M.Sc. Thesis, Arizona State University, Tempe, AZ

Tsai TL, Chiang SJ (2013) Modeling of layered infinite slope failure triggered by rainfall. Environ Earth Sci 68(5):1429–1434

Tsai TL, Yang JC (2006) Modeling of rainfall-triggered shallow landslide. Environ Geol 50:525–534

Vanapalli SK, Fredlund DG (2000) Comparison of different procedures to predict the shear strength of unsaturated soils uses the soil-water characteristic curve. Geo-Denver 2000, American Society of Civil Engineers, Special Publication, no 99, pp 195–209

Vanapalli SK, Fredlund DG, Pafahl DE, Clifton AW (1996) Model for the prediction of shear strength with respect to soil suction. Can Geotech J 33:379–392

Varnes DJ, IAEG Commission on Landslides and other Mass-Movements (1984) Landslide hazard zona-
    tion: a review of principles and practice. The UNESCO Press, Paris, p 63
Wang C, Li S, Esak T (2008) Natural hazards and earth system sciences GIS-based two-dimensional numer-
    ical simulation of rainfall-induced debris flow. Nat Hazards Earth Syst Sci 8:47–58
Wieczorek GF (1987) Effect of rainfall intensity and duration on debris flows in central Santa Cruz Moun-
    tains, California. In: Costa JE, Wieczorek GF (eds) Debris flows/avalanches: processes, recognition
    and mitigation, Reviews in Engineering Geology, Geological Society of America, no 7, pp 23–104
Wieczorek GF, Naeser ND (2000) Proceedings of the second international conference on debris-flow haz-
    ards mitigation: mechanics, prediction, and assessment. In: Balkema AA (ed), Rotterdam, p 212
Zapata CE (1999) Uncertainity in soil-water characteristic curve and impacts on unsaturated shear strength
    prediction. Ph.D. Dissertation, Arizona State University, Tempe, United States
Zezere JL, Trigo RM, Trigo IF (2005) Shallow and deep landslides induced by rainfall in the Lisbon region
    (Portugal): assessment of relationships with the North Atlantic Oscillation. Nat Hazards Earth Syst Sci
    5:331–344
Zhang LL, Zang J, Zang LM, Tang WH (2011) Stability of analysis of rainfall induced slope failure: a
    review, Geotechnical Engineering, Vol 164 Issue GE5, Institute of Civil Engineers Geotechnical Engi-
    neering 164 October 2011 Issue GE5